RSC Advances

ROYAL SOCIETY OF CHEMISTRY

www.rsc.org/advances

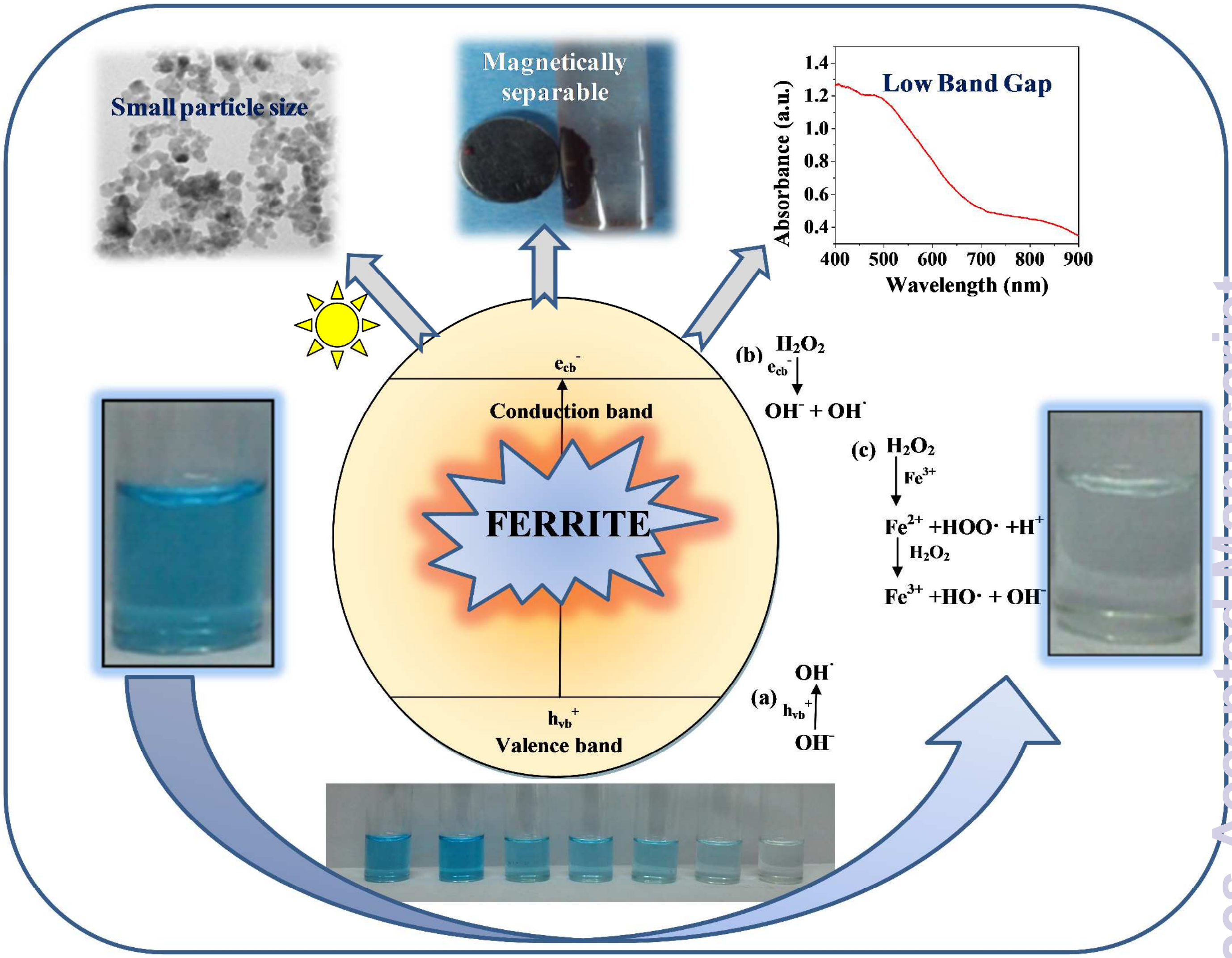
Small particle size
Magnetically separable
Low Band Gap
Absorbance (a.u.)
1.4
1.2
1.0
0.8
0.6
0.4
400
500
600
700
800
900
Wavelength (nm)
e_{cb}^{-}
Conduction band
FERRITE
h_{vb}^{+}
Valence band
(b) H_2O_2 $\xrightarrow{e_{cb}^{-}}$ $OH^{-} + OH^{\cdot}$
(c) H_2O_2 $\xrightarrow{Fe^{3+}}$ $Fe^{2+} + HOO\cdot + H^{+}$ $\xrightarrow{H_2O_2}$ $Fe^{3+} + HO\cdot + OH^{-}$
(a) OH^{-} $\xrightarrow{h_{vb}^{+}}$ $OH^{\cdot}$

Tailoring the photo-Fenton activity of spinel ferrites (MFe_2O_4) by incorporating different cations(M=Cu, Zn, Ni and Co) in the structure.

Rimi Sharma[1], S. Bansal[2] and SonalSinghal[*1]
[1]Department of Chemistry, Panjab University, Chandigarh, India-160014.
[2]DST, New Delhi
[*]**sonal1174@gmail.com**

Abstract

Magnetic bimetallic nanospinels (MFe_2O_4; M=Cu, Zn, Ni and Co) of size ranging between 15-30 nm were synthesized by facile and viable sol-gel method. The analysis of Fourier Transform Infrared Spectra of all the samples demonstrated formation of M-O bond in spinel structure. Structural exploration of all the nano materials using Powder X-Ray Diffraction and High Resolution Transmission Electron Microscopy revealed formation of single phase cubic spinel structure. All the materials exhibited magnetic temperament with high surface area (92-151 m^2/g). Furthermore, band gap calculated from diffuse reflectance spectra was quite narrow (1.26-2.08eV) for all the samples, hence ferrites could act as visible light driven photocatalyst. The prepared nanospinels were proposed to be promising heterogeneous photo-Fenton catalyst under visible light for the degradation of organic pollutants. The catalytic results revealed that rate of reaction was significantly influenced by the cation in the spinel structure as degradation order was observed to be $CuFe_2O_4$ (k=0.286 min^{-1}) >$ZnFe_2O_4$ (k=0.267 min^{-1}) > $NiFe_2O_4$(k=0.138 min^{-1}) > $CoFe_2O_4$ (k=0.078 min^{-1}). The reaction conditions were optimized for all the ferrites as the photodegradation was influenced by ferrite dosage (0.25-1.00 g/L), pH (2-5) and H_2O_2 concentration (4-27 mM). The experimental data disclosed that activity of ferrite was sensitive to sintering temperature. The materials displayed remarkable stability in the reaction as it could be magnetically separated using external magnet and recycled up to 4 consecutive cycles. There was no significant loss in activity of all the material demonstrating an excellent ability of ferrites to remove organic pollutants from wastewater.

Key Words: Photodegradation; Heterogeneous catalyst; Photo-Fenton; Spinel ferrites

Introduction

In the present scientific world development of environmentally benign catalyst is of significant importance. The most vital feature of a green catalyst for its industrial application is its capability to be efficiently recovered after the reaction.[1]The conventional catalyst isolation methods such as chromatography, filtration, centrifugation etc. are monotonous and cause a lot of inconvenience.[2] To overcome these issues, the concept of magnetically separable nanocatalysts is emerging to be a robust and highly efficient alternative. The inherent magnetic characteristic of these materials allows simple and efficient separation from the reaction mixture thereby minimizing the required work up procedures.[3]Consequently the sustainability of magnetic catalyst satisfies the principles of green chemistry.

In the class of magnetic nanomaterials, magnetite (Fe_3O_4) is one of the simplest ferrospinel[4] that has attracted considerable attention and is being intensely investigated in different reactions. The properties of magnetite are engineered by introduction of cation such as Co, Ni, Cu, Mn, Zn etc. in its structure. These modified ferrospinels commonly known as ferrites have general formula MFe_2O_4 (M=Co, Ni, Cu, Zn, Mn). In ferrites, substitution of iron with second metal improves the properties as well as catalytic scopewhile iron component enables magnetic recovery of catalyst after the reaction.[5]Spinel ferrites are emerging as focus of recent scientific research due to its excellent catalytic performance in reactions such as CO_2 reduction[6], coupling reactions[7], methane oxidative conversion[8], water gas shift reaction[9], adsorbent for removal of toxic substances[10] etc.

These materials have a relevant characteristic of narrow band gap which lies in the visible region.[11]This property allows ferrites to efficiently utilize the visible region of the solar spectrum in the photocatalytic reactions such as oxidative dehydrogenation of hydrocarbons[12], decomposition of H_2O_2[13], degradation of different organic pollutants[14-16]etc. In addition to these applications ferrites can be used as a potential photo-Fenton catalyst as they enhance oxidizing power of Fenton type reactions. Hitherto, many authors have dedicated there research for degradation of organic pollutants in aqueous solutions using ferrites. For instance, researchershave illustrated the role of zinc ferrite ($ZnFe_2O_4$) nanoparticles in photodegradation of different dyes under visible light.[17,18]Mahmoodi observed low performance for photodegradation of Reactive Red 198 (RR198) and Reactive Red 120 (RR120) in the absence of ferrite.[17]Mesoporous $ZnFe_2O_4$ was employed by Su et al. for photocatalytic degradation of Acid Orange II (AOII) dye under visible light/H_2O_2 system.[18]Similarly monodisperse cobalt ferrite ($CoFe_2O_4$) nanoparticles of 2-6 nm size were employed by Feng et. alfor degradation of methylene blue dye.[19] The use of bismuth ferrite ($BiFeO_3$) for photodegradation reactions has been explored by different researchers.[20-22]

To the best of our knowledge, no research has been carried out on modulating the photo-Fenton activity by altering the cation within the ferrite. In this context, herein we report a simple and facile fabrication of spinel ferrites (MFe_2O_4; M=Cu, Zn, Ni and Co) using sol-gel methodology. The prepared materials were characterized using diverse techniques. The application of these materials was demonstrated in the heterogeneous photo-Fenton degradation reaction. In the present study, Methylene blue (MB) dye was used as a model pollutant. The properties of ferrites strongly depend on the cation present in the spinel structure; hence the present aim is to study comparative effect of different ferrites for the degradation reaction. The influence of various parameters such as catalyst loading, dye concentration, initial pH of dye solution, annealing temperature and H_2O_2 concentration on the degradation reaction in the presence of all the ferrites was studied. Furthermore, verification of main active species responsible for degradation i.e. hydroxyl radical ($^{\cdot}OH$) was also investigated. In the end, the recyclability of catalyst was evaluated for 4 consecutive cycles without any significant loss in activity indicating stability of material.

2. Experimental Section

2.1 Materials

Ferric nitrate ($Fe(NO_3)_3.9H_2O$, 98%), cupric nitrate ($Cu(NO_3)_2.3H_2O$, 99.5%), nickel nitrate ($Ni(NO_3)_2.6H_2O$, 98%), zinc nitrate ($Zn(NO_3)_2.6H_2O$, 96%), cobalt nitrate ($Co(NO_3)_2.6H_2O$, 99%), citric acid (99.57%) and hydrogen peroxide (30% w/v) were procured from Fisher Scientific. Ethylene glycol (99%) and methylene blue were supplied by Merck and CDH respectively. All the chemicals were of analytical grade, commercially available and used without further purification.

2.2 Synthesis of ferrite

Ferrites with general formula MFe_2O_4 (M=Co, Ni, Zn, Cu) were synthesized using modification of previously reported sol-gel method.[23,24] In a typical procedure to synthesize $ZnFe_2O_4$, stochiometric amount of zinc nitrate (0.02 moles, 5.949 g) and ferric nitrate (0.04 moles, 16.16 g) were dissolved in minimum amount of distilled water with magnetic stirring at

80-90 °C. After complete dissolution, citric acid (in the molar ratio 1:1 to precursor metal salts) and ethylene glycol (10 ml) were added into the above solution and stirred until gel formation. The gels were dried and crushed to obtain ferrite powder. Finally annealing was carried out at 400 °C and 1000 °C for 2 hours in muffle furnace before further characterization and application. Similar procedure was followed for synthesis of other ferrites.

2.3Photocatalytic activity

Photocatalyticperformance of prepared ferrites was evaluated by degradation of MB in aqueous solution. All the experiments were performed at room temperature under ambient conditions. For degradation reactions, stock solution of 10 mg/L MB was prepared in distilled water.In all the experiments the molar ratio of H_2O_2/MB/ferrite was fixed at 1/0.001/0.065.In a typical reaction, desired amount (25-100 mg) of ferrite nanoparticles was dispersed in 100 ml of MB solution (pH-2.5 using H_2SO_4). Prior to irradiation under Xe-lamp, the suspension was magnetically stirred in dark for 30 minutes, followed by addition of H_2O_2. 3 ml aliquots of dye solution were taken out at regular time intervals and catalyst was separated. The change in concentration of degraded solution was analyzed using UV-Vis spectroscopy. The photo degradation study was performed by varying different reaction conditions such as catalyst loading, dye concentration, pH, H_2O_2 dosage and annealing temperature under similar reaction conditions.

2.4Physical characterization

Thermogravimetric analysis was performed by heating the raw samples on a thermalanalyzer, SDT Q 600 with a heating rate of 10 °C/min. Formation of M-O bond in ferrites was detected using Fourier Transform Infrared Spectrophotometer (PERKIN ELMER) in the range 800-400 cm^{-1}. High Resolution Transmission Electron Microscope (FEI Tecnai, G2 F20) with an accelerating voltage of 200keV was used to calculate the particle size of photocatalyst.Phase purity and structural propertyof samples was investigated using X-Ray diffractometer (model Bruker AXS, D8 advance) with radiation of Cu target (Cu K_{α}= 1.54 Å). Optical properties were probed by diffuse reflectance spectroscopy by means of UV-Vis absorption (Ana-lytikjena specord-205) spectrophotometer. Magnetic characterization as a function of magnetic field (±10 kOe) wasscrutinizedat room temperature using Vibrating Sample

Magnetometer (155,PAR).The Brunauer-Emmett-Teller (BET)surface area analyzer ((11-2370) Gemini, Micromeritics, USA) was used to measure the surface area. A 150 W Xe-lamp with 96000 Lux was used as a visible light source. The concentration of MB was analyzed using UV-Vis spectrophotometer (JASCO, V-530).

3.1 Characterization of catalysts

3.1.1 Thermogravimetric Analysis (TGA)

The combustion process of all the as prepared ferrite samples was investigated using TGA. The typical TGA curves of as obtained $NiFe_2O_4$shown in Fig. SF1 (supporting information)exhibited decomposition in two weight loss steps. The first stage was observed around 50-100 °C owing to loss of water molecules from the sample. The second weight loss in the range of 300-400 °C was ascribed to the decomposition of ethylene glycol and nitrates into CO_2 and NO_x respectively.[25, 26] When the temperature was increased beyond 400 °C, no further weight loss was observed indicating formation of pure $NiFe_2O_4$. Similar TGA curves were obtained for rest of the ferrite samples. Therefore all the ferrite samples were sintered at minimum temperature of 400 °C before characterization.

3.1.2 Fourier Transform Infrared Spectroscopy (FTIR)

The peaks in the FTIR spectra are due to vibration of ions in crystal lattice. Formation of metal-oxygen (M-O) bond in ferrites was supported by this study. The room temperature FTIR spectra of all the ferrites annealed at 400 °C and 1000 °Cis shown in Fig. SF2 (A) and (B) respectively (supporting information).Both the graphs depicted two vibration bands in the range of 600-400 cm^{-1}forall the ferrites. The band at higher frequency(ν_{tet}) was assigned to stretching vibration between tetrahedral metal ions and oxygen ion (M_{tet}-O), while the band at lower frequency (ν_{oct}) was attributed to stretching vibration of bonds between octahedral metal ions and oxygen ion (M_{oct}-O).[27]

3.1.3 High Resolution Transmission Electron Microscopy (HRTEM)

HRTEM was used to examine the size, distribution and crystallanity of particles in all the ferrites. The synthesized sample was dispersed in absolute ethanol and few drops of dispersion were placed on carbon grid in order to obtain HRTEM images. The typical low resolution TEM micrograph of $CuFe_2O_4$ obtained after annealing at 400 °C is shown in Fig. 1 (a). The results indicated that the particles were highly agglomerated due to magnetic characteristic of ferrites.[28]The average particle size was around 15 nm which was consonant with the results of XRD. In a similar manner the particle size of other ferrites were obtained and are listed in Table ST1 (supporting information).

Particle size of samples crucially depends on temperature of heat treatment. An increase in particle size was observed in case of sample annealed at higher temperature due to fusion of neighboring particles. The TEM image of $CuFe_2O_4$ annealed at 1000 °C is given in Fig. 1 (b). The image indicated enhancement in the particle size with increasein annealing temperature from 400 °C to 1000 °C. Such increase in particle size with annealing temperature was consistent with the earlier reports.[29]

HRTEM study revealed that all the nanoparticles were crystallized into single crystals of ferrite. The HRTEM images of $CuFe_2O_4$ nanoparticles at magnification of 2 nm and 5 nm are shown in Fig 1 (c) and (d) respectively. The crystallite planes were judged from the measured average fringe width values labeled on the HRTEM image. The average fringe width calculated from the profile of frame (Fig. 1(e)) was observed to be 0.25 nm corresponding to (311) plane whichis the most intense peak obtained in XRD. The live FFT of $CuFe_2O_4$ is given in inset of Fig. 1 (c) and the reconstructed image after filtering FFT pattern of HRTEM is given in Fig. 1 (f).

3.1.4 Powder X-Ray diffraction (XRD) studies

The crystal structure, phase purity and crystallite size of the synthesized nano ferrites was investigated using Powder XRD. The XRD patterns of all the ferrites annealed at 400 and 1000 °Care shown in Fig. 2.For all the ferrites annealed at 400 °C, diffraction peaks corresponding to (hkl) (220), (311), (400), (511) and (440) planes can be readily indexed to formation of single phase cubic spinel structureaccording to the JCPDS card no. 01-089-1012, 00-001-1121, 01-077-0010 and 00-003-0875 for $ZnFe_2O_4$, $CoFe_2O_4$, $CuFe_2O_4$ and $NiFe_2O_4$ respectively.A close examination of XRD patterns illustrated that peak intensity gradually increased and became narrow with increase in annealing temperature from 400 °C to 1000 °C. Thus the samples became crystalline with annealing. All the ferrites were stable to heat treatment as cubic spinel structure was retained in case of $ZnFe_2O_4$, $CoFe_2O_4$ and $NiFe_2O_4$. However in case of $CuFe_2O_4$ spinel structure got transformed into tetragonal. Such transformation of structure in case of $CuFe_2O_4$ has been reported in literature.[30]

The crystallite size was calculated using most intense peak broadening of 311 plane with the help of Debye Scherer formula.[31] The values of crystallite size for the samples annealed at 400 °C varied between 15-30 nm and are given in Table ST1 (supporting information). Lattice parameter for all the ferrites annealed at 400 °C were calculated using Le-Bail refinement method and were in the range of 8.35-8.44 Å which is in consistence with earlier reported values (Table ST1, supporting information).[32-34]

3.1.5 Optical properties

Optical property is key factor in designing highly efficient photocatalyst. The typical UV-Vis Diffuse Reflectance Spectrum of $ZnFe_2O_4$presented in Fig. 3 (a) demonstrated absorption edge around 730 nm illustrating its suitability for visible light photocatalysis. The ferrites could absorb considerable amount of visible light due to electron excitation from O-2p level (valence band) to Fe-3d level (conduction band).[35]The optical band gap was estimated by using following equation.[15]

$$\alpha h\nu = A(h\nu - E_g)^{n/2} \tag{1}$$

where α is the absorption coefficient, ν is the light frequency, E_g is the band gap, h is Plank's contant and A is a constant. The bandgap calculated from the plot of $(\alpha h\nu)^2$*versus*hν (photon energy) was 1.94 eV(Fig.3 (b)) which is in close agreement with the value reported in literature.[11] Similarly band gap of rest of the materials were calculated and the values varied between 1.26-2.08 eV(Table ST1, supporting information). The band gap values were quite narrow hence all the ferrites could act as visible light driven photocatalyst.

3.1.6Magnetic Study

Magnetic characteristic of material is a crucial property which is determined by recording magnetization curves at room temperature using Vibrating Sample Magnetometer (VSM). The hysteresis loop of all the samples annealed at 400 °C shown in Fig. 4 clearly illustrated their magnetic behavior. Different parameters such as saturation magnetization (M_s) and coercivity(H_c) deduced from the magnetization curves are listed in Table ST1(supporting information). From the figure and values listed in Table it is clear that coercivity of $CoFe_2O_4$ is very high as compared to other samples, which is a typical behavior of hard ferrites. Therefore it can be concluded that $CoFe_2O_4$ is a hard ferrite while rest of the samples come under the category of soft ferrites.

Furthermore, the M_s of $CoFe_2O_4$ and $CuFe_2O_4$ is much higher than other two samples (M_s is 6, 19, 60 and 65 emu/g for $ZnFe_2O_4$, $NiFe_2O_4$, $CuFe_2O_4$ and $CoFe_2O_4$ respectively). In addition to this, it was observed that saturation magnetization at nano range is lower as compared to its bulk counterpart which may be due to small size, surface disorder and modified cation distribution at nano level.[36] From this study it is concluded that all the ferrites can be magnetically separated from the reaction mixture using external magnet for many cycles without any significant loss.

3.1.7 BET Surface Area Analysis

The surface area of all the synthesized spinel ferrites was estimated using Brunauer-Emmett-Teller (BET) surface analyzer at -196 °C. The sample was prepared at 150 °C for 2 hours with the flow of N_2 gas. The concept of BET is an extension of Langumir theory and is based on BET equation proposed by Brunauer, Emmett and Teller.[37]

$$\frac{1}{Q\left[\left(\frac{P_0}{P}\right)-1\right]} = \frac{C-1}{Q_m C}\left(\frac{P}{P_0}\right) + \frac{1}{Q_m C} \qquad (2)$$

where P is the equilibrium pressure, $P_0$is the saturation pressure, Q is thequantity of the gas adsorbed on the adsorbate, Q_m is themonolayer adsorbed gas quantity and C is the BET constant. The BET plots ($1/[Q(P_0/P)]$ vs P/P_0) of all the samples are given in Fig. 5. The plots were observed to be linear and unique values of Q_m and C were estimated from slope (A) and intercept (I) according to the equations given in supporting information.Different variables calculated from BET plots such as slope, intercept, Q_m, C, S_{total} and S_{BET} are listed in Table 1. The values of BET surface area of all the synthesized samples were found to be in the range of 92-151 m^2/g.

3.2 Photocatalytic Activity

Photo-Fenton activity was investigated by measuring the rate of degradation of aqueous MB solution in the presence of ferrite under visible light irradiation. The UV-Vis spectrum of MB contained 4 absorption peaks at 664 nm, 617 nm, 292 nm and 246 nm. The essential peak at 664 nm was in the visible region with a shoulder at 617 nm and the other two peaks were in the UV region. The major band at 664 nm appeared due to conjugation between two dimethylamine substituted aromatic rings through S and N and the peaks in ultra violet region were assigned to aromatic rings.[38, 39]

3.2.1 Control experiment

Various control experiments were designed for the degradation of MB in the presence of all the ferrites. The typical results of $NiFe_2O_4$are illustrated in Fig. 6 A. Under visible light irradiation MB exhibited ~10% decomposition (Fig. 6 A (a)) while no significant degradation of MB was observed in the absence of ferrite ($MB+H_2O_2$ only) both under dark as well as in the presence of light (Fig. 6 A (b), (c)). Experiments were also carried out in the absence of H_2O_2 (MB+ferrite only) both under dark and light. The results showed no appreciable degradation with time (Fig. 6 A (d), (e)). In the absence of light ($MB+H_2O_2$+ferrite) although ~30% degradation was observed (Fig. 6 A (f)), but the degradation was greatly enhanced to ~99% in the presence of light (Fig. 6 A (g)). Hence presence of light, ferrite and H_2O_2 were necessary for photo-fenton like degradation of MB. The control experiments were performed for all the ferrites and similar results were observed.

Fig. 6 B shows the typical absorption spectra of MB in the presence of $NiFe_2O_4$ nanoparticles. When H_2O_2 was added to MB solution peak at 246 nm was masked due to absorption of H_2O_2 in this region. The absorption maxima gradually dropped in intensity with increasing irradiation time without the appearance of any new band in the UV or visible region. The rapid decrease in intensity of absorption band indicated break down of chromophore structure responsible for the color of dye. The percentage of dye degraded can be calculated using following equation.[40]

$$\% \, degradation = \frac{C_0 - C_t}{C_0} \times 100 \tag{3}$$

where C_0 is initial MB concentration and C_t is the concentration at time t.

3.2.2 Kinetics of photocatalytic degradation

The photocatalytic degradation of MB in the presence of MFe_2O_4 (M=Co, Ni, Cu, Zn) followed pseudo first order kinetics and could be expressed according to Langumir Hinshelwood (L-H) model.[39, 41]

$$r = -\frac{dC}{dt} = \frac{k_r k_{LH} C}{1+K_{LH}C} \tag{4}$$

where r ($mgL^{-1}min^{-1}$) is rate of reaction , k_r ($mgL^{-1}min^{-1}$) is reaction rate constant, K_{LH} (Lmg^{-1}) is adsorption a rate constant, C (mgL^{-1}) is reactant concentration and t (min) is the time of irradiation. In the present reaction initial concentration of MB was low; therefore rate could be expressed as:

$$r = -\frac{dC}{dt} = \frac{k_r K C}{1+K_{LH}C} = kC \tag{5}$$

where k (min^{-1}) is pseudo first order rate constant and by integrating in limit of $C=C_0$ at t=0, equation (5) can be expressed as:

$$ln\frac{C_0}{C} = kt \tag{6}$$

The plot of ln (C_0/C) vs t for all the ferritesis shown in Fig. 7 and rate constant of the reaction obtained from the slope are tabulated in Table 2.

3.2.3 Factors influencing photocatalytic degradation

(a) Catalyst Loading

Catalyst loading is one of the important parameters in photocatalytic process. Therefore experiments were carried out to assess an optimum amount of catalyst dosage for the reaction. Investigations of MFe_2O_4 (M = Cu, Zn, Ni, Co) concentration on the photodegradation of MB dye by varying amount of catalyst from 0.25g/L-1g/L at constant dye concentration of 10 mg/L, H_2O_2-8mM and pH-2.5 was performed. All the reactions followed pseudo first order kinetics and the rate constants are tabulated in Table 2. It was interesting to note that in the initial stages with increase in the dosage of catalyst, the rate of reaction increased, however, after a certain value it declined. The initial elevation in rate of reaction may be due to increase in total active sites on the surface of catalyst, when the catalyst exceeded optimum value, rate constant dropped due to increase in turbidity of solution which caused reduction in light penetration through the solution.[41, 42]On the basis of above observations all the experiments were performed with 0.5g/L of photocatalyst.

(b) Dye concentration

The initial MB concentration has significant effect on rate of photodegradation and this was determined for all the ferrites by varying dye concentration from 10-30 mg/L at constant catalyst loading of 0.5 g/L, pH-2.5, H_2O_2-8 mM.Photodegradation of MB in the presence of all the ferritesat different dye concentration is shown in Fig. 8. The observed results revealed decrease in rate of degradation with increase in dye concentration. This could be explained by the fact that there was limited production of hydroxyl radical ($OH^{\cdot}$) in the solution while the number of dye molecules was increasing causing reduction in rate of reaction. Another reason might be explained by Beer-Lambert law according to which as the initial dye concentration was increased, path length of photons entering the solution decreased resulting in decrease of rate.[43]

(c) H_2O_2 dosage

The influence of H_2O_2 concentration on the rate of degradation of MB in the presence of all the ferrites was investigated by varying H_2O_2 dosage from 4 mM to 27 mM. Fig. 9 shows the variation in the values of rate constants with H_2O_2 concentration in the presence of the ferrites. It was observed that the value of rate constant initially increased with increase in concentration of H_2O_2 up to 8 mM and then decreased. The initial increase was expected due to the reaction of H_2O_2 with ferrite to yield $OH^{\cdot}$. However addition of large amount of oxidant may cause scavenging of $OH^{\cdot}$, thus decreasing not only the rate of reaction but also leading to wastage of H_2O_2.[44]

$$OH^{\cdot} + H_2O_2 \rightarrow H_2O + HOO^{\cdot} \qquad (7)$$

$$HOO^{\cdot} + OH^{\cdot} \rightarrow H_2O + O_2 \qquad (8)$$

In order to achieve higher degradation rate of MB, the concentration of H_2O_2 should be optimum and was fixed at 8 mM.

(d) Variation of pH

The pH of solution is one of the significant factors in photo-Fenton like degradation of dye and this effect was studied for all the ferrites. Fig. 10 shows the effect of pH (range 2-5) on degradation of MB in the presence of all the ferrites by heterogeneous photo-Fenton like process. It was seen that the removal efficiency was ~99% at pH 2.5 and an increase in the pH of solution lead to decrease in removal efficiency. This outcome might be due to formation of Fenton's reagent at lower pH to generate $OH^{\cdot}$ (hydroxyl radical) which are the main active species for the degradation of dye.[45] Therefore, the initial pH was adjusted to 2.5 for further experiments.

(e) Effect of annealing temperature

Photocatalytic activity of metal oxide nano particles is strongly influenced by particle size, morphology and surface area. Jadhav et al. have reported the effect of sintering temperature on photodegradation of methyl orange using $ZnFe_2O_4$.[46] Fig. 11 displayed the concentration curves of MB in the presence of all four ferrites annealed at 400 °C and 1000 °C. The results indicated that the samples annealed at 400 °C had higher efficiency as compared to the samples annealed at 1000 °C. The decrease in photocatalytic activity of the samples annealed at 1000 °C might be attributed to increase in particle size and decrease in surface area with increase in annealing temperature. This increase in particle size was confirmed from TEM study.

3.2.4 Mechanism of photodegradation

The possible mechanism for photodegradation of MB over MFe_2O_4 (M= Co, Ni, Cu, Zn) is outlined in Fig. 12 (A) The active species for photodegradation of dye could be produced by 3 pathways:-

When ferrite was irradiated in the presence of visible light electron/hole (e^-/h^+) pair was generated on the surface (equation 9)

$$MFe_2O_4 + h\nu \rightarrow MFe_2O_4\ (e_{CB}^- + h_{VB}^+) \tag{9}$$

(i) The photogenerated hole h_{VB}^+ could react with water or hydroxyl ion (H_2O or OH^-) to generate hydroxyl radical (equation 10, 11).

$$h_{VB}^+ + H_2O \rightarrow H^+ + OH^{\cdot} \tag{10}$$

$$h_{VB}^{+} + OH^{-} \rightarrow OH^{\cdot} \quad (11)$$

(ii) The photogenerated electron e_{CB}^{-} could be captured by H_2O_2 to yield $OH^{\cdot}$, limiting the recombination of holes and electron thus enhancing the photocatalytic activity.

$$H_2O_2 + e_{CB}^{-} \rightarrow OH^{-} + OH^{\cdot} \quad (12)$$

(iii) The reaction of H_2O_2 with Fe(III) (on the surface of ferrite) and Fe(II) generated Fenton reagent which produced hydroxyl radical.

$$Fe^{3+} + H_2\,O_2 \rightarrow Fe^{2+} + HOO^{\cdot} + H^{+} \quad (13)$$

$$Fe^{2+} + H_2\,O_2 \rightarrow Fe^{3+} + OH^{\cdot} + OH^{-} \quad (14)$$

Since $OH^{\cdot}$ was produced by 3 pathways, enhancement in rate of degradation was observed. The hydroxyl radical produced by above 3 pathways was the main active species for degradation of MB.

Verification of mechanism

To evaluate the role of $^{\cdot}OH$ in the mechanism, the photodegradation reaction was carried out in the presence of a known $^{\cdot}OH$ scavenger i.e. isopropyl alcohol (IPA). Fig. 13 shows the effect on the rate constant values when the reaction was carried out in the presence and absence of scavenger. The results indicated degradation rate was markedly depressed when IPA was added to reaction mixture suggesting that the main active species during the reaction was $^{\cdot}OH$.

3.2.5Comparitive study of MFe_2O_4 (M=Zn, Cu, Ni and Co) for the degradation of MB

Under optimum reaction conditions ([ferrite]-0.5 g/L, [MB]-10 mg/L, pH-2.5, $[H_2O_2]$-8 mM), the degradation of MB was carried out using all the ferrites annealed at 400 °C. The order of reactivity evaluated from rate constant values (Table 2) was $CuFe_2O_4 > ZnFe_2O_4 > NiFe_2O_4 > CoFe_2O_4$.

The generation of Fenton reagent can be tuned by substitution of transition metals such as Cu, Zn, Ni and Co in Fe_3O_4. The catalytic activity in case of ferrites is mainly due to metal ions in octahedral sites. The mechanism of electron transfer is given in Fig. 12 (B). The cations in the octahedral site accelerated the electron transfer to regenerate Fe^{2+} hence increasing the catalytic activity.

In case of $CuFe_2O_4$, very high activity is observed. This may be attributed to the fact that Cu^{2+} can also produce Fenton like reagent as demonstrated in following equations.[47]

$$Cu^{+} + H_2O_2 \rightarrow Cu^{2+} + OH^{\cdot} + OH^{-} \qquad (15)$$

$$Cu^{2+} + H_2O_2 \rightarrow Cu^{+} + HOO^{\cdot} + H^{+} \qquad (16)$$

The formation of Cu^{+}/ Cu^{2+} redox pair causes formation of more number of $OH^{\cdot}$ radicalsleading to high activity of $CuFe_2O_4$.

This order can be related with the band gap of ferrites. It is well known from literature that lower the band gap higher the photocatalytic activity. This trend was followed in case of all the ferrites except cobalt ferrite. The band gap of cobalt ferrite was lowest however its photocatalytic activity was least. This might be due to recombination of photogenerated e^{-}/h^{+} pair. It was also observed that the activity of ferrites does not depend on the surface area calculated from BET. The catalytic activity of ferrites can also be correlated with the magnetization values. Based on charge and size metal ions possess an inherent character to occupy either tetrahedral or octahedral site of the ferrite sub lattice. The catalytic activity of ferrites is also due to metal ions in octahedral sites. The high activity of $CuFe_2O_4$ can be correlated to the tendency of Cu^{2+} to occupy octahedral site[48] which enables easy electron exchange between variable oxidation states of Cu.

3.2.6 Contrast of synthesized photocatalyst with literature precedents

A detailed literature review illustrated use of different photocatalysts for the degradation of MB.[49-53] Hence comparison of photodegradation efficiency of various photocatalyst with the present system was done and is shown in Table 3. Entries in Table 3 clearly demonstrate superiority of synthesized spinel ferrites in terms of photocatalytic performance. In addition to this, all the synthesized materials possessed advantages of being stable, magnetically recoverable and recyclable after the reaction without any significant loss in activity.

3.2.7Recyclability

Stability and recyclability of the photocatalyst is of prime importance for its potential application in long term process to decompose organic pollutants that are present in waste water. Ferrites possess heterogeneous photo-Fenton like activity and excellent magnetic properties; hence can be easily separated from the reaction mixture using external magnet. After the completion of reaction, the catalyst was magnetically separated, washed 5 times with distilled water followed by drying in oven at 100 °C. The recovered catalyst was again redispersed in fresh MB solution for next cycle. All the ferrite nanoparticles did not exhibit any significant loss of activity even after four cycles demonstrating high stability of the synthesized photo catalyst, hence confirming their promising application in waste water treatment. The typical degradation percentage of MB in the presence of all the ferrites for 4 successsive cycles is shown in Fig. 14.

4. Conclusion

To conclude visible light active nanospinels MFe_2O_4 (M=Ni, Cu, Zn, Co) were successfully fabricated via sol-gel method for photo-Fenton like degradation of MB. The formulated ferrites in the nano range were well characterized by various techniques. The present study revealed role of cation in the degradation process as the most effective catalyst out of all the four ferrites was $CuFe_2O_4$ (~ 99% degradation in 15 min) followed by $ZnFe_2O_4$, $NiFe_2O_4$ and $CoFe_2O_4$ respectively. Optimum reaction conditions were determined and an investigation of kinetics revealed that the reactions follow pseudo first order. The prepared materials possessed excellent magnetic properties thus leading to its easy separation from aqueous solution by external magnet without bringing into play additional filtration step. Furthermore, the results indicated that the catalyst could be reused up to four cycles without any significant loss of activity hence envisaging its potential application for photo-Fenton like degradation of organic pollutants from wastewater.

Acknowledgments

The authors are highly grateful to DST (SERB) and Council of Scientific and Industrial Research (CSIR) for providing the necessary financial support.

References

1. D. Wang and D.Astruc, *Chem. Rev.*,2014, **114**, 6949−6985.

2. L.M. Rossi, N.J.S. Costa, F.P. Silva and R. Wojcieszak, *Green Chem.*, 2014, **16**, 2906-2933.
3. T. Cheng, D. Zhang, H. Li and G. Liu, Green Chem., 2014, **16**, 3401-3427.
4. K. Lazar, T. Mathew, Z. Koppany, J. Megyeri, V. Samuel, S.P. Mirajkar, B. S. Rao and L. Guczi, *Phys. Chem. Chem. Phys.*, 2002, **4**, 3530-3536.
5. R. Hudson, Y. Feng, R.S. Varma and A. Moores, *Green Chem.*, 2014, **16**, 4493-4505,
6. C.S. Hwang and N.C. Wang, *Mater. Chem. Phy.*, 2004, **88**, 258-263.
7. A.S. Singh, S.S. Shendage and J.M. Nagarkar, *Tetrahedron Lett.*, 2013, **54**, 6319-6323.
8. F. Papa, L. Patron, O. Carp, C. Paraschiv and B. Ioan, *J. Mol. Catal. A: Chem.*, 2009, **299**, 93-97.
9. J. Tsagaroyannis, K.J. Haralambous, Z. Loizos, G. Petroutsos and N. Spyrellis, *Mater. Lett.*,1996, **28**, 393-400.
10. Y.J. Tu, C.F. You, C.K. Chang, S.L. Wang and T.S. Chan, *Chem. Eng. J.*, 2013, 225, 433-439.
11. E. Casbeer, V.K. Sharma and X.Z. Li, *Sep. Purif. Technol.*, 2012, **87**, 1-14.
12. M.A. Gibson and J.W. Hightower, *J. Catal.*, 1976, **41**, 420-430.
13. M.I. Zaki, W. Ramadan, Ali Katrib, A.I.M. Rabee, *App. Surf. Sci.*, 2014, **317**, 929-934.
14. X. Li, Y. Hou, Q. Zhao, W. Teng, X. Hua and G. Chen, *Chemosphere*, 2011, **82**, 581-586.
15. X. Li, Y. Hou, Q. Zhao and L. Wang, *J. Colloid Interf. Sci.*, 2011, **358**, 102-108.
16. Y. Sun,W. Wang, L. Zhang, S. Sun and E. Gao, *Mater. Lett.*,2013, 98, 124-127.
17. N.M. Mahmoodi, *Mater. Res. Bull.*, 2013, **48**, 4255-4360.
18. M. Su, C. He, V.K. Sharma, M.A. Asi, D. Xia, X.Z. Li, H. Deng and Y. Xiong, *J. Hazard. Mater.* , 2012, **211– 212**, 95-103.
19. X. Feng, G.Y. Mao, F.X. Bu, X.L. Cheng, D.M. Jiang and J.S. Jiang, *J. Magn. Magn. Mater.*, 2013, **343**, 126-132.
20. W. Wang, N. Li, Y. Chi, Y. Li, W. Yan, X. Li and C. Shao, *Ceram. Int.***,** 2013, **39**, 3511-3518.
21. J. An, L. Zhu, Y. Zhang and H. Tang, *J. Envirn. Sci.*, 2013, **25(6)**, 1213-1225.
22. W. Luo, L. Zhu, N. Wang, H. Tang, M. Cao, and Y. She. *Environ. Sci. Technol.*, 2010, **44**, 1786-1791.

23. M. Sajjia, M. Oubaha, M. Hasanuzzaman A.G. Olabi, *Ceram. Int.*, 2014, **40**, 1147-1153.
24. G.B. Teh, Y.C. Wong and R.D. Tilley, *J. Magn. Magn. Mater.*, 2011, **323**, 2318-2322.
25. S. Sutradhar, S. Pati, S. Acharya, S. Das, D. Das and P.K. Chakrabarti, *J. Magn. Magn. Mater.*, 2012, **324**, 1317-1325.
26. P. Sivakumar, R. Ramesh, A. Ramanand, S. Ponnusamy and C. Muthamizhchelvan, *Appl. Surf. Sci.*, 2012, **258**, 6648-6652.
27. T. Slatineanu, A.R. Iordan, M.N. Palamaru, O.F. Caltun, V. Gafton and L. Leontie, *Mater. Res. Bull.*,2011,**46**, 1455-1460.
28. M.A. Gabal, R.S. Al-luhaibi and Y.M. Al Angari, *J. Hazard. Mater.*, 2013, **246–247**, 227-233.
29. M.G. Naseri, E.B. Saion, H.A. Ahangar, M. Hashim and A.H. Shaari, *J. Magn. Magn. Mater.*, 2011, **323**, 1745-1749.
30. S. Kimura, T. Mashino, T. Hirokia, D. Shigeoka, N. Sakai, L. Zhu and Y. Ichiyanagi. *ThermochimActa*, 2012, **532**, 119-122.
31. P. Pascuta, A. Vladescu, G. Borodi, E. Culea and R. Tetean, *Ceram. Int.*, 2011, **37**, 3343-3349.
32. A. Hassadee, T. Jutarosaga and W. Onreabroy, *Procedia Engineering*, 2012, **32**, 597-602.
33. A.I. Nandapure, S.B. Kondawar, P.S. Sawadh and B.I. Nandapure, *Physica B*, 2012, **407**,1104-1107.
34. M. Ajmal and A. Maqsood, *J. Alloy. Compd.* 2008, **460**, 54-59.
35. P. Guo, G. Zhang, J. Yu, H. Li and X.S. Zhao,*Coll. Surf. A*, 2012, **395**, 168-174.
36. S.A. Saafan, S.T. Assar, B.M. Moharram and M.K. El Nimr, *J. Magn. Magn. Mater.*, 2010, **322**, 628-632.
37. A.K. Ladavos, A.P. Katsoulidis, A. Iosifidis, K.S. Triantafyllidis, T.J. Pinnavaia and P.J. Pomonis, *MicroporousMesoporous Mater.*, 2012, **151**, 126-133.
38. M.A. Rauf, M.A. Meetani, A. Khaleel and A. Ahmed, *Chem. Eng. J.*, 2010, **157**,373-378.
39. T. Soltani and M.H. Entezari, *J. Mol. Catal. A-Chem.*, 2013, **377**, 197-203.
40. T. Xie, L. Xu, C. Liu and Y. Wang, *Appl. Surf. Sci.*, 2013, **273**, 684-691.
41. T. Soltani and M.H. Entezari, *Ultrason. Sonochem.*, 2013, **20**, 1245-1253.
42. K.N. Harish, H.S.B. Naik, P.N.P. Kumar and R. Viswanath, *ACS Sustainable Chem. Eng.*, 2013, **52**, 8174-8181.

43. M.H. Habibi, N. Talebian and J.H. Choi, *Dyes Pigments*, 2007, **73**, 103-110.
44. F.D. Mai, C.C. Chena, J.L. Chen and S.C. Liu, *J. Chromatogr. A*, 2008, **1189**,355-365.
45. B. Sahoo, S.K. Sahu, S. Nayak, D. Dhara and P. Pramanik, *Catal. Sci. Technol.* 2012,**2**, 1367-1374.
46. S.D. Jadhav, P.P. Hankare, R.P. Patil and R. Sasikala, *Mater. Lett.* 2011, **65**, 371-373.
47. X. Zhang, Y. Ding, H. Tang, X. Han, L. Zhu and N. Wang,*Chem. Eng. J.*, 2014, **236**, 251-262.
48. S. Bhukal, Shivali and S. Singhal, *Mater. Sci. Semicond. Process.*, 2014, 26, 467-476.
49. M. BoraAkinn and M. Oner, *Ceram. Int.*, 2013, **39**, 9759–9762.
50. X. Li, C. Hu, X. Wang and Y. Xi, *Appl. Surf. Sci.*, 2012,**258**, 4370–4376.
51. N. Talebian and M.R. Nilforoushan, *Thin Solid Films*, 2010, **518**, 2210–2215.
52. N. Raghavan, S. Thangavel and G.Venugopal, *Mater. Sci. Semicond. Process.* 2015, **30**, 321–329.
53. R. Chauhan, A. Kumar, R.P. Chaudhary, *J. Lumin.*, 2014, **145**, 6–12.

Table 1 Different parameters calculated from BET plot of all the ferrites annealed at 400 °C

Ferrite	Slope (g/cm^3)	Intercept (g/cm^3)	Q_m (cm^3/g)	C	S_{total} (m^2/g)	S_{BET} (m^2/g)
$CuFe_2O_4$	0.099205	0.000599	10.0196	166.600191	~43	~97
$ZnFe_2O_4$	0.078485	0.000446	12.6693	176.966319	~55	~151
$NiFe_2O_4$	0.11805	0.001056	8.9976	105.259751	~40	~92
$CoFe_2O_4$	0.081386	0.000481	12.2149	170.076638	~53	~137

Table 2 Variation of rate constant with catalyst loading in the presence of all ferrites

Ferrite	Catalyst Loading (g/L)			
	0.25	**0.50**	**0.75**	**1.00**
$CuFe_2O_4$ k (min^{-1})	0.226	0.286	0.071	0.037
$ZnFe_2O_4$ k (min^{-1})	0.224	0.267	0.218	0.105
$NiFe_2O_4$ k (min^{-1})	0.089	0.138	0.130	0.103
$CoFe_2O_4$ k (min^{-1})	0.076	0.078	0.054	0.050

Table 3 Comparative results of the synthesized ferrite with photocatalyst reported in literature for degradation of MB

S.No.	Photocatalyst	Concentration of MB	Time (min)	% degradation	Reference No.
1.	Sphere like ZnO	5 mg/L	1103	97	48
2.	CdS nanoparticles	4 mg/L	140	76	49
3.	In_2O_3 thin films	5 mg/L	240	85	50
	ZnO thin films		240	55	
	SnO_2 thin films		240	38	
	TiO_2 thin films		240	70	
4.	Reduced graphene oxide/TiO_2/ZnO	0.3 mg/L	120	92	51
5.	Cu doped ZnS	10 mg/L	180	100	52

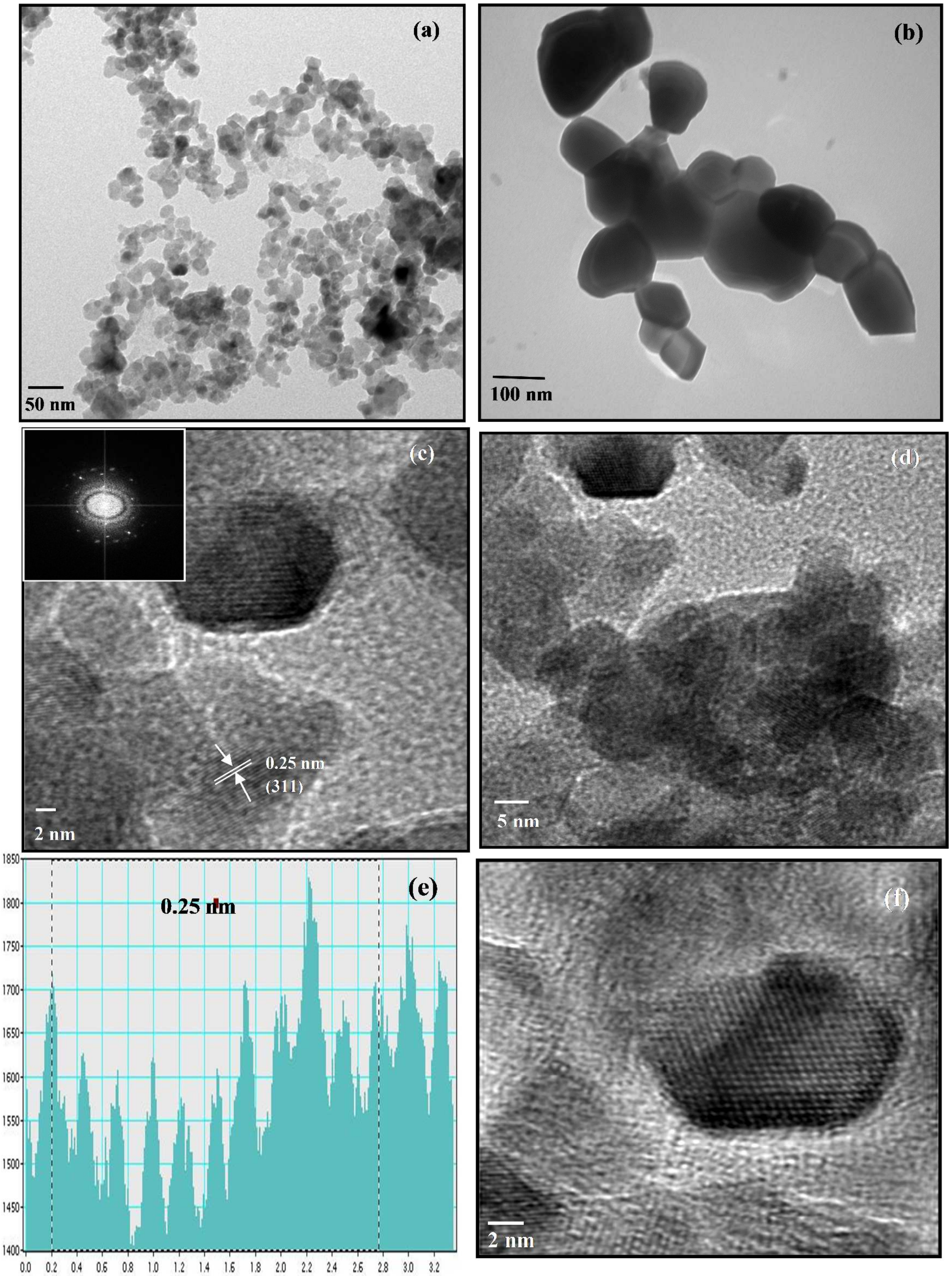

Fig. 1 TEM image of $CuFe_2O_4$ annealed at (a) 400 °C and (b) 1000 °C, HRTEM image of $CuFe_2O_4$ nanoparticles at (c) magnification of 2 nm (inset shows FFT of $CuFe_2O_4$) and (d) magnification of 5 nm (e) profile of frame for the average fringe width (f) reconstructed image after filtering FFT pattern of HRTEM.

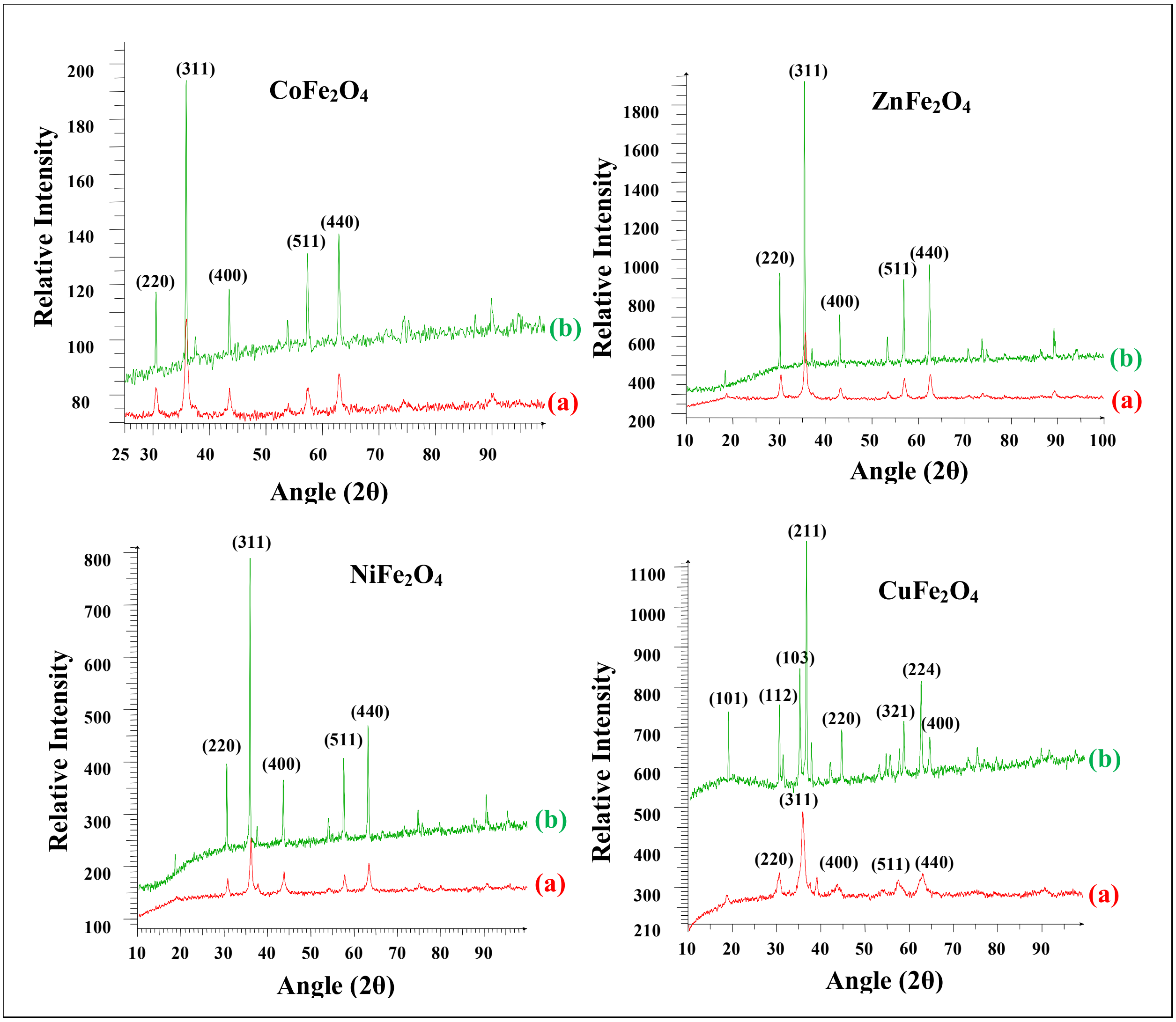

Fig. 2 Powder X-Ray Diffractographs of all the ferrites annealed at (a) 400 °C and (b) 1000 °C.

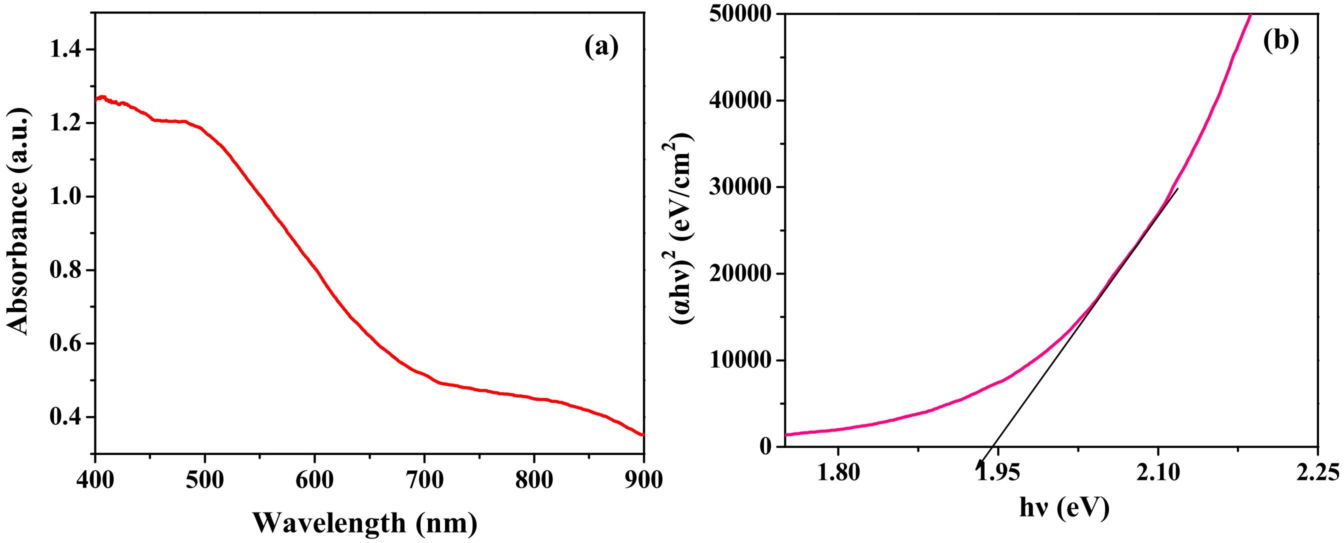

Fig. 3 (a) Diffuse reflectance spectra and (b) $(\alpha h\nu)^2$vshν plot of the $ZnFe_2O_4$annealed at 400 °C

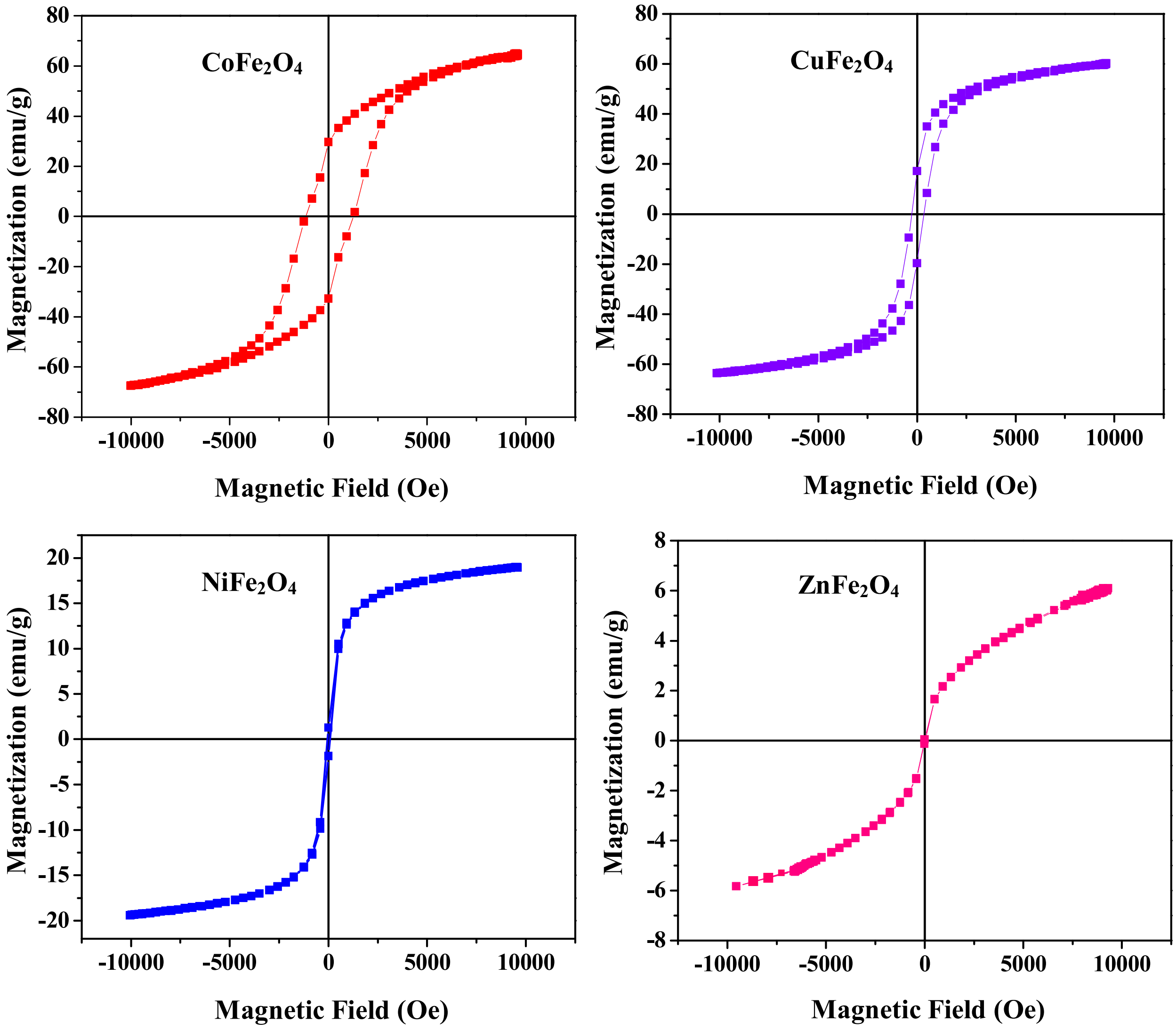

Fig. 4Magnetic hystersis loop of all the ferrites annealed at 400 °C

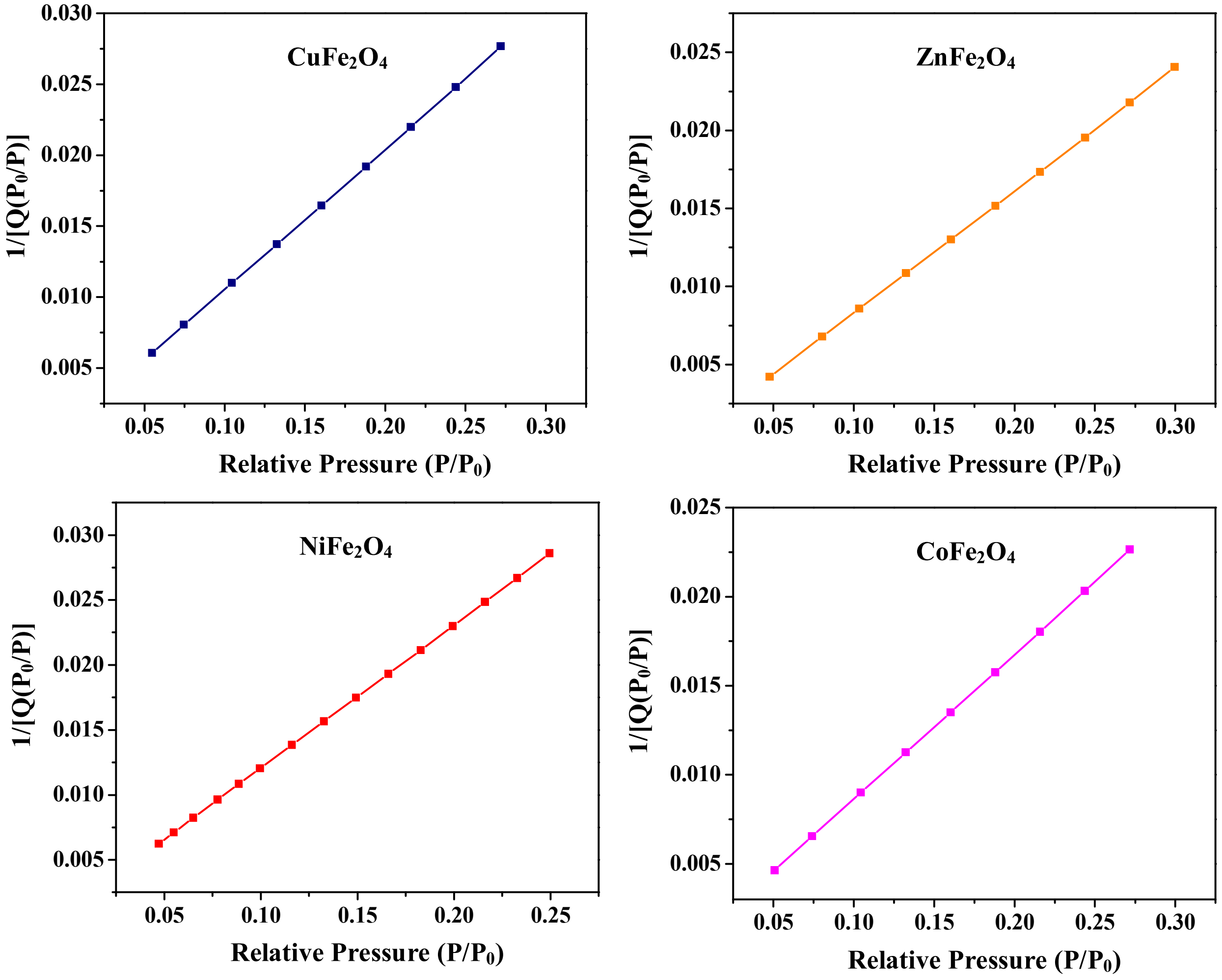

Fig.5 BET plots of all the ferrites annealed at 400 °C

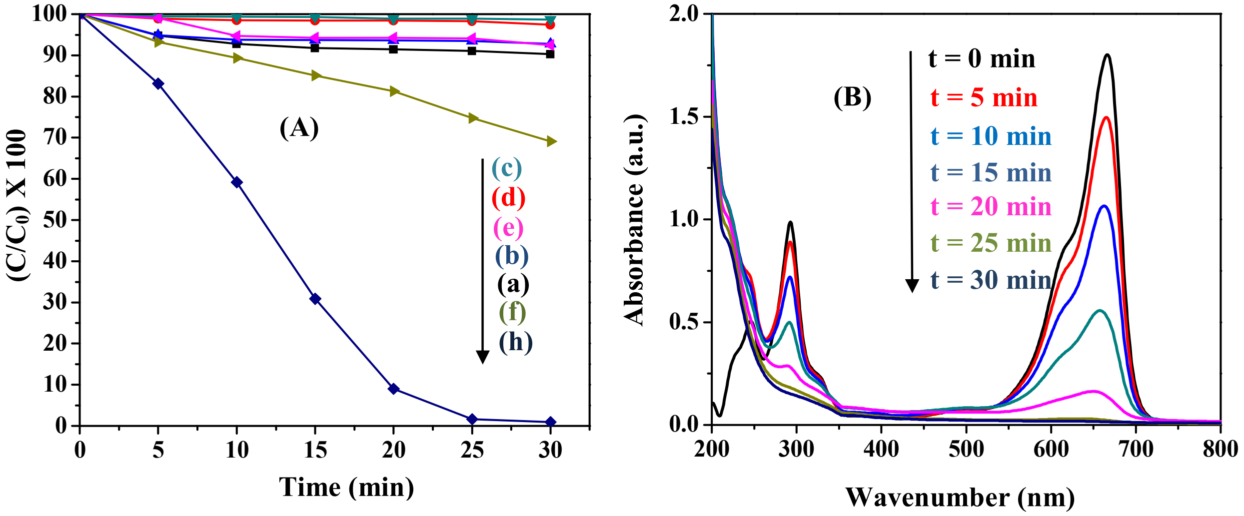

Fig. 6 A Control experiments for photocatalytic degradation in the presence of $NiFe_2O_4$.The reaction conditions are (a) MB+light (c) MB+H_2O_2+dark (d) MB+H_2O_2+light (e) MB+ferrite+dark (f) MB+ferrite+light (g) MB+ferrite+H_2O_2+dark (h) MB+ferrite+H_2O_2+light.

B Change in absorption spectra of MB with time in the presence of $NiFe_2O_4$ (0.5 g/l), pH-2.5, H_2O_2-8 mM.

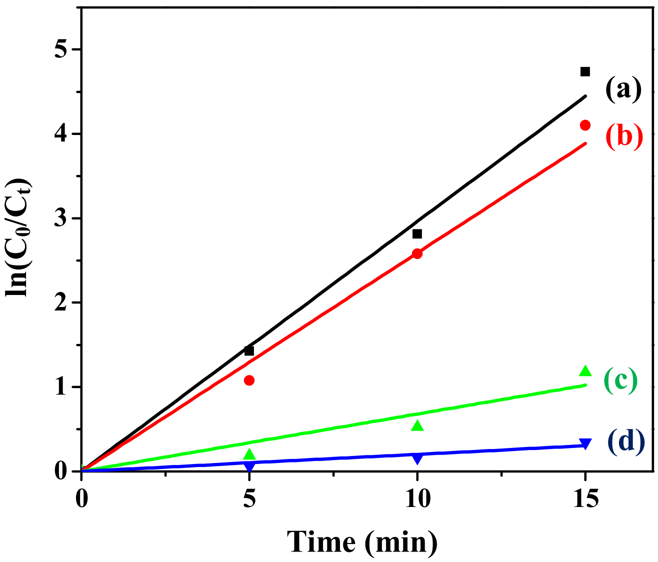

Fig. 7 Photodegradation kinetics of MB in the presence of (a) $CuFe_2O_4$ (b) $ZnFe_2O_4$ (c) $NiFe_2O_4$ and (d) $CoFe_2O_4$ under optimum conditions

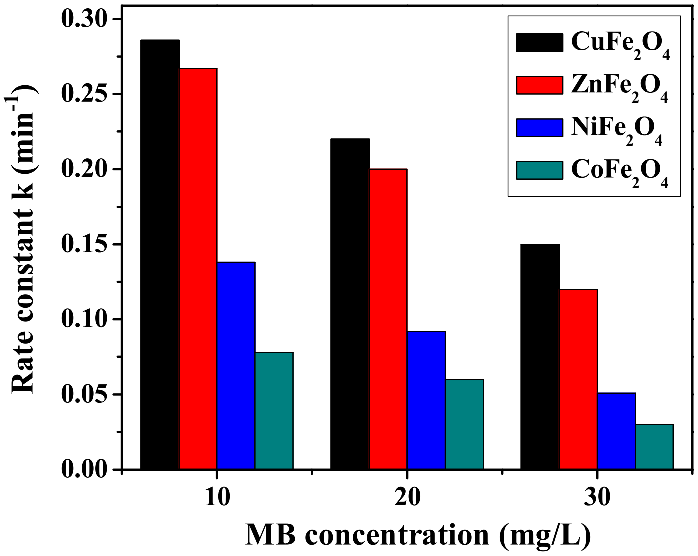

Fig.8 Photodegradationrate of MB in the presence of all the ferrites at different dye concentrations

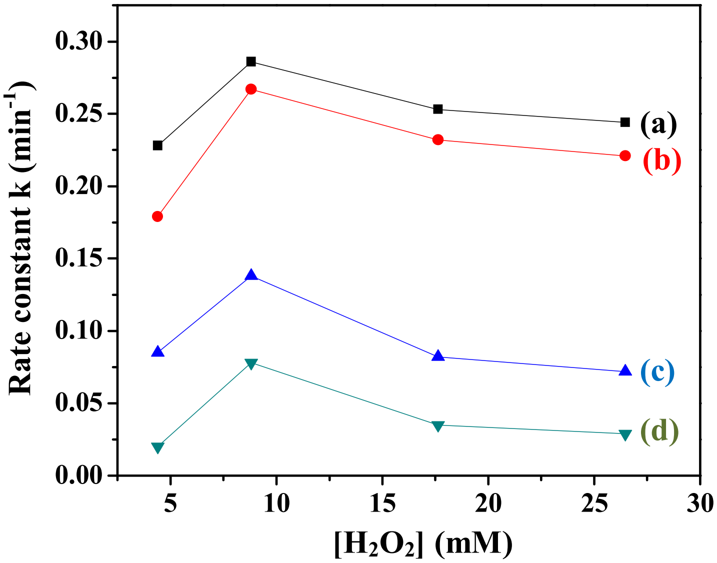

Fig.9 Variation of rate constant with [H_2O_2] in the presence of (a) $CuFe_2O_4$ (b) $ZnFe_2O_4$(c) $NiFe_2O_4$ and (d) $CoFe_2O_4$

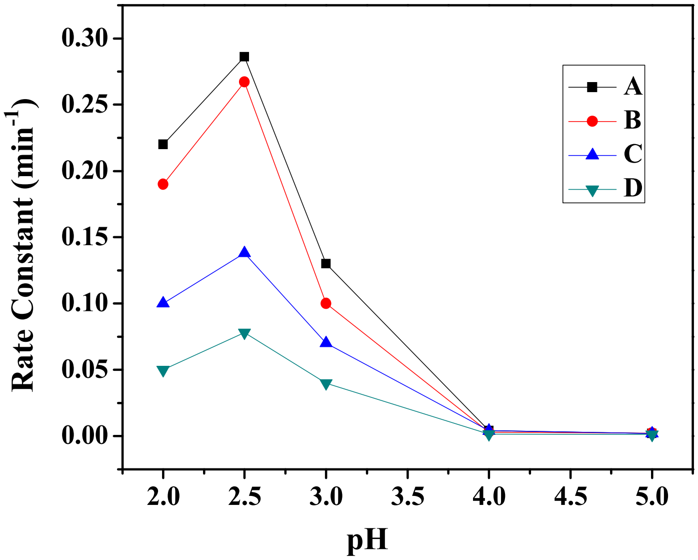

Fig. 10 Effect of pH on the rate constant values in the presence of (A) $CuFe_2O_4$ (B) $ZnFe_2O_4$ (C) $NiFe_2O_4$ and (D) $CoFe_2O_4$

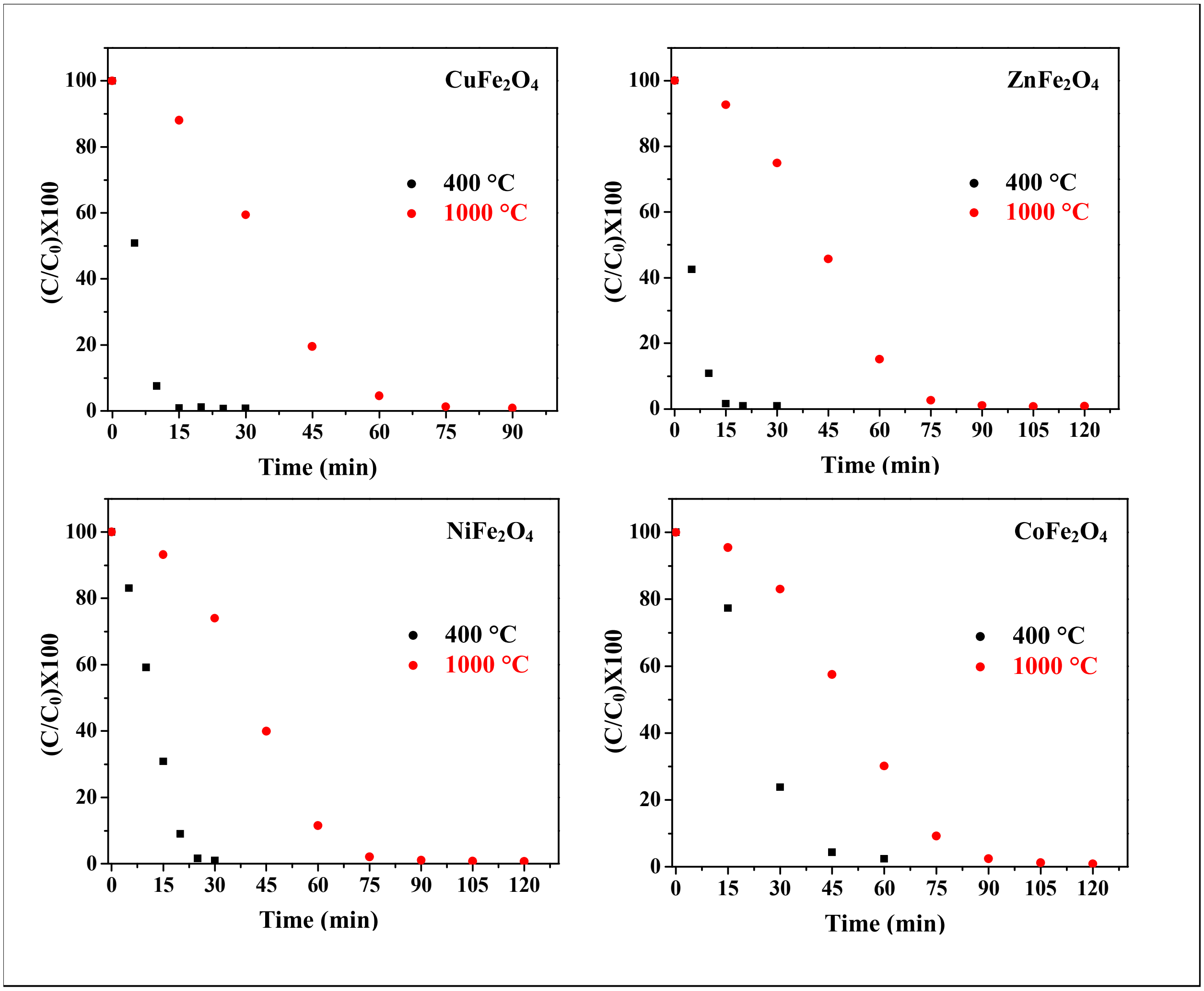

Fig. 11 Effect of annealing temperature on photocatalytic activity of all the ferrites

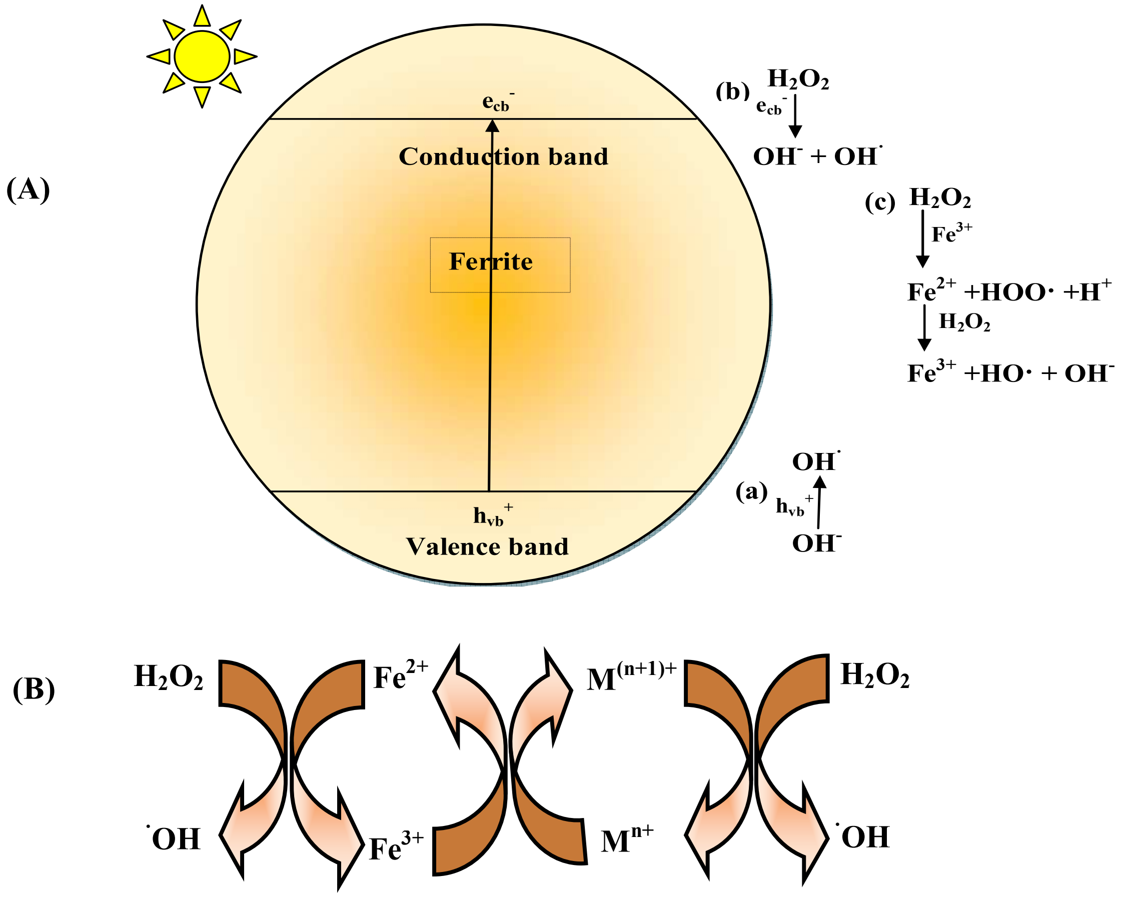

Fig. 12 Mechanism of generation of hydroxyl radical (OH·) in the presence of ferrite/H_2O_2/light system

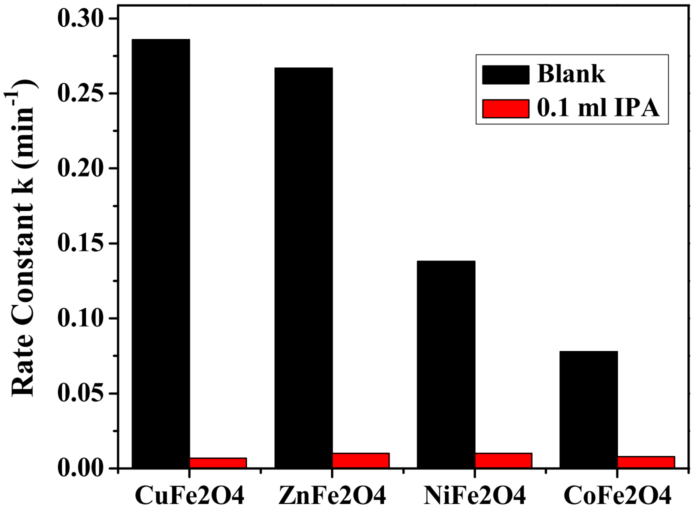

Fig. 13 Effect of addition IPA on the degradation reactions in the presence of all the ferrites

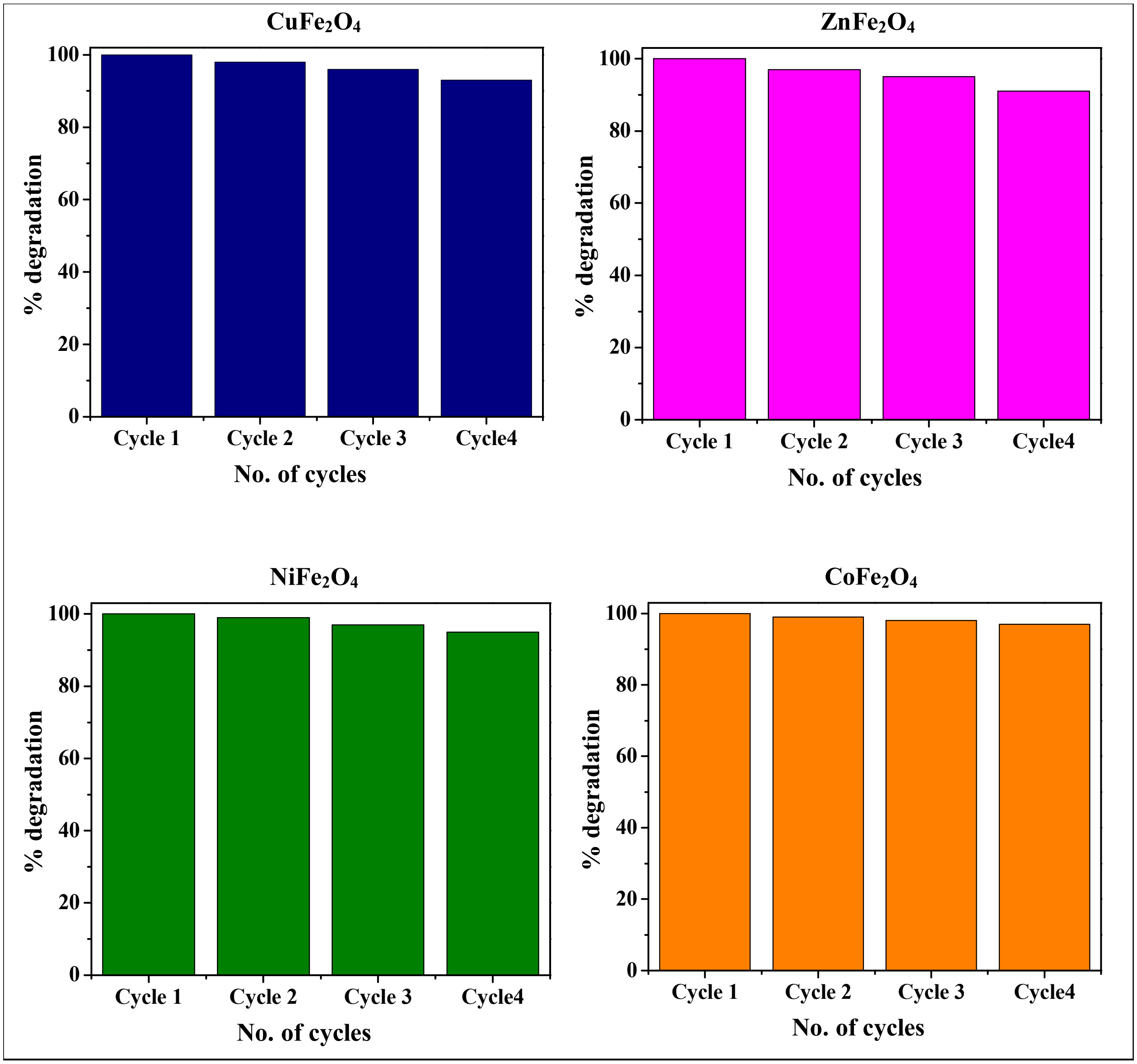

Fig. 14 Reusability of all the ferrites for 4 successive cycles under similar conditions